AECE | ADVANCES IN ELECTRICAL AND COMPUTER ENGINEERING

Universitatea Ştefan cel Mare Suceava

PUBLISHER

Stefan cel Mare
University of Suceava

Faculty of Electrical
Engineering and
Computer Science

13, Universitatii Street
Suceava - 720229
ROMANIA

Print ISSN: 1582-7445
Online ISSN: 1844-7600
WorldCat: 643243560
doi: 10.4316/AECE

TABLE OF CONTENTS - Current Issue

Issue: **1**, Volume: **21**, Year: **2021**
Published Online: **February 2021**
Acceptance Rate: **20%**
Number of Papers in this Issue: **11**
Web of Science® Times Cited: **0** (Citations/Papers: **0.000**)
SCOPUS® Times Cited: **0** (Citations/Papers: **0.000**)

Comparative Analysis of Permanent Magnet Synchronous Generators with Mechanical Energy Storage according to Machine Types

PARK, Y.-S.
Publication Year: 2021, Page(s): 3 - 10
Digital Object Identifier: 10.4316/AECE.2021.01001
Web of Science® Times Cited: n/a - SCOPUS® Times Cited: n/a

AbstractPlus | Citation | Quick view | Download PDF (2,419 KB)

File System Performance Comparison in Full Hardware Virtualization with ESXi, KVM, Hyper-V and Xen Hypervisors

DJORDJEVIC, B., TIMCENKO, V., KRALJEVIC, N., MACEK, N.
Publication Year: 2021, Page(s): 11 - 20
Digital Object Identifier: 10.4316/AECE.2021.01002
Web of Science® Times Cited: n/a - SCOPUS® Times Cited: n/a

AbstractPlus | Citation | Quick view | Download PDF (1,402 KB)

A New Visual Cryptography Method Based on the Profile Hidden Markov Model

OZCAN, H., KAYA GULAGIZ, F., ALTUNCU, M. A., ILKIN, S., SAHIN, S.
Publication Year: 2021, Page(s): 21 - 36
Digital Object Identifier: 10.4316/AECE.2021.01003
Web of Science® Times Cited: n/a - SCOPUS® Times Cited: n/a

AbstractPlus | Citation | Quick view | Download PDF (2,981 KB)

Phase-Locked Loop with Inverse Tangent based Phase Detection

STOJIC, D.
Publication Year: 2021, Page(s): 37 - 44
Digital Object Identifier: 10.4316/AECE.2021.01004
Web of Science® Times Cited: n/a - SCOPUS® Times Cited: n/a

AbstractPlus | Citation | Quick view | Download PDF (1,404 KB)

A Semi-automatic Heart Sounds Identification Model and Its Implementation in Internet of Things Devices

JUSAK, J., PUSPASARI, I., KUSUMAWATI, W. I.
Publication Year: 2021, Page(s): 45 - 56
Digital Object Identifier: 10.4316/AECE.2021.01005
Web of Science® Times Cited: n/a - SCOPUS® Times Cited: n/a

LINKS

AECE on Wikipedia
DAS Conference
DAS on Wikipedia
EMCLab Laboratory
Hard & Soft Contest

TEXT LINKS

Anycast DNS Hosting

AbstractPlus | Citation | Quick view | Download PDF (3,956 KB)

Interference, Traffic Load and Delay Aware Routing Metric for Wireless Mesh Network

BHOJANNAWAR, S., MANGALWEDE, S.
Publication Year: 2021, Page(s): 57 - 64
Digital Object Identifier: 10.4316/AECE.2021.01006
Web of Science® Times Cited: n/a - SCOPUS® Times Cited: n/a

AbstractPlus | Citation | Quick view | Download PDF (1,210 KB)

Data-Driven Predictive Control of a Pneumatic Ankle Foot Orthosis

ULKIR, O., AKGUN, G., NASAB, A., KAPLANOGLU, E.
Publication Year: 2021, Page(s): 65 - 74
Digital Object Identifier: 10.4316/AECE.2021.01007
Web of Science® Times Cited: n/a - SCOPUS® Times Cited: n/a

AbstractPlus | Citation | Quick view | Download PDF (1,450 KB)

Continuous Student Knowledge Tracing Using SVD and Concept Maps

TEODORESCU, O. M., POPESCU, P. S., MOCANU, L. M., MIHAESCU, M. C.
Publication Year: 2021, Page(s): 75 - 82
Digital Object Identifier: 10.4316/AECE.2021.01008
Web of Science® Times Cited: n/a - SCOPUS® Times Cited: n/a

AbstractPlus | Citation | Quick view | Download PDF (1,420 KB)

Fuzzy Contrast Enhancement System with Multiple Transform Domain Operations

JAVID, T., ABID, M.
Publication Year: 2021, Page(s): 83 - 90
Digital Object Identifier: 10.4316/AECE.2021.01009
Web of Science® Times Cited: n/a - SCOPUS® Times Cited: n/a

AbstractPlus | Citation | Quick view | Download PDF (2,167 KB)

Lossy Compression using Adaptive Polynomial Image Encoding

OTHMAN, S., MOHAMED, A., ABOUALI, A., NOSSAIR, Z.
Publication Year: 2021, Page(s): 91 - 98
Digital Object Identifier: 10.4316/AECE.2021.01010
Web of Science® Times Cited: n/a - SCOPUS® Times Cited: n/a

AbstractPlus | Citation | Quick view | Download PDF (1,465 KB)

Generating Manageable Electricity Demand Capacity for Residential Demand Response Studies by Activity-based Load Models

SONMEZ, M. A., BAGRIYANIK, M.
Publication Year: 2021, Page(s): 99 - 108
Digital Object Identifier: 10.4316/AECE.2021.01011
Web of Science® Times Cited: n/a - SCOPUS® Times Cited: n/a

AbstractPlus | Citation | Quick view | Download PDF (1,828 KB)

SAFFARIAN, A.
Issue 4/2020
AbstractPlus

Wavelet-Based Adaptive Anisotropic Diffusion Filter, TANYERI, U., DEMIRCI, R.
Issue 4/2018
AbstractPlus

Expansible Network-on-Chip Architecture, PIRES, I. L. P. ALVES, M. A. Z., ALBINI, L. P.
Issue 2/2018
AbstractPlus

A Semi-automatic Heart Sounds Identification Model and Its Implementation in Internet of Things Devices, JUSAK, J., PUSPASARI, I., KUSUMAWATI, W. I.
Issue 1/2021
AbstractPlus

Model-based Dynamic Fractional-order Sliding Mode Controller Design for Performance Analysis and Control of a Coupled Tank Liquid-level System, SEKBAN, H. T., CAN, K., BASCI, A.
Issue 3/2020
AbstractPlus

TOP ARTICLES

Most cited in WOS »
Most cited in SCOPUS »
Most read articles »

LATEST NEWS

2020-Jun-29
Clarivate Analytics published the InCites Journal Citations Report for 2019. The InCites JCR Impact Factor of Advances in Electrical and Computer Engineering is **1.102** (**1.023** without Journal self-cites), and the InCites JCR 5-Year Impact Factor is **0.734**.

2020-Jun-11
Starting on the 15th of June 2020 we will introduce a new policy for reviewers. Reviewers who provide timely and substantial comments will receive a discount voucher entitling them to an APC reduction. Vouchers (worth of 25 EUR or 50 EUR, depending on the review quality) will be assigned to reviewers after the final decision of the reviewed paper is given. Vouchers issued to specific individuals are not transferable.

2019-Dec-16
Starting on the 15th of December 2019 all paper authors are required to enter their SCOPUS IDs. You may use the free **SCOPUS ID lookup form** to find yours in case you don't remember it.

2019-Jun-20
Clarivate Analytics published the InCites Journal Citations Report

for 2018. The JCR Impact Factor of Advances in Electrical and Computer Engineering is **0.650**, and the JCR 5-Year Impact Factor is **0.639**.

2018-May-31
Starting today, the minimum number a pages for a paper is 8, so all submitted papers should have 8, 10 or 12 pages. No exceptions will be accepted.

Read Mor

HelpDesk

AECE | ADVANCES IN ELECTRICAL AND COMPUTER ENGINEERING

Universitatea Ştefan cel Mare Suceava

PUBLISHER

Stefan cel Mare University of Suceava

Faculty of Electrical Engineering and Computer Science

13, Universitatii Street
Suceava - 720229
ROMANIA

Print ISSN: 1582-7445
Online ISSN: 1844-7600
WorldCat: 643243560
doi: 10.4316/AECE

EDITORIAL BOARD

EDITOR-IN-CHIEF

Adrian GRAUR
Stefan cel Mare University of Suceava, Romania

ASSOCIATE EDITORS

Mihai DIMIAN
Stefan cel Mare University of Suceava, Romania

Ioan DUMITRACHE
Romanian Academy, Romania

Florin Gheorghe FILIP
Romanian Academy, Romania

Aurelian ROTARU
Stefan cel Mare University of Suceava, Romania

Radu-Daniel VATAVU
Stefan cel Mare University of Suceava, Romania

EXECUTIVE EDITOR

Eugen COCA
Stefan cel Mare University of Suceava, Romania

INTERNATIONAL SCIENTIFIC BOARD MEMBERS

Dumitru N. ALEXANDRU
Technical University Iasi, Romania

Petru ANDREI
Florida State University, United States of America

Dragan ANTIC
University of Nis, Serbia

Oleg BREKHOV
Moscow Aviation Institute, Russia

Mihai CERNAT
Transilvania University Brasov, Romania

Christophe CHAILLOU
University of Science and Technology, Lille, France

Hariton Nicolae COSTIN
University of Medicine and Pharmacy Iasi, Romania

Gary FRIEDMAN
Drexel University, Philadelphia, United States of America

Timothy HALL
University of Limerick, Ireland

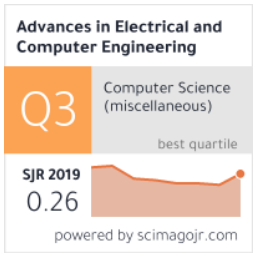

FORMER EDITORIAL BOARD MEMBERS

LATEST NEWS

2020-Jun-29
Clarivate Analytics published the InCites Journal Citations Report for 2019. The InCites JCR Impact Factor of Advances in Electrical and Computer Engineering is **1.102** (**1.023** without Journal self-cites), and the InCites JCR 5-Year Impact Factor is **0.734**.

2020-Jun-11
Starting on the 15th of J 2020 we wiil introduce a policy for reviewers. Revie who provide timely and substantial comments will receive a discount voucher entitling them to an APC reduction. Vouchers (worth of 25 EUR or 50 EUR, depending on the review quality) will be assigned to reviewers after the final decision of the reviewed paper is given. Vouchers issued to specific individuals are not transferable.

2019-Dec-16
Starting on the 15th of December 2019 all paper authors are required to enter their SCOPUS IDs. You may use the free **SCOPUS ID lookup form** to find yours in case you don't remember it.

2019-Jun-20
Clarivate Analytics published the InCites Journal Citations Report for 2018. The JCR Impact Factor of Advances in Electrical and Computer Engineering is **0.650**, and the JCR 5-Year Impact Factor is **0.639**.

2018-May-31
Starting today, the minimum number a pages for a paper is 8, so all submitted papers should have 8, 10 or 12 pages. No exceptions will be accepted.

Read More »

FORMER INTERNATIONAL SCIENTIFIC BOARD MEMBERS

Alexei POKROVSKII †
National University of Ireland, Cork, Ireland

Ileana HAMBURG
Institute for Work and Technology, Gelsenkirchen, Germany

John MILNER †
City University of London, Great Britain

Nicola PITRONE
University of Catania, Italy

Fedir SOPRONIUC
Yuriy Fedkovych Chernivtsi University, Ukraine

Mircea STRATULAT
Politehnica University of Timisoara, Romania

Gavril TODEREAN
Technical University of Cluj-Napoca, Romania

DTP & ON-LINE PUBLISHING

Eugen COCA
Stefan cel Mare University of Suceava, Romania

A Semi-automatic Heart Sounds Identification Model and Its Implementation in Internet of Things Devices

Jusak JUSAK, Ira PUSPASARI, Weny Indah KUSUMAWATI
Dept. of Computer Engineering, Dinamika University, Surabaya, Indonesia
jusak@dinamika.ac.id

***Abstract*—Identification of heart sound signals in the form of a phonocardiogram (PCG) has recently attracted the attention of many researchers along with the development of small devices and global Internet connection in a way to offer automatic illness detection and monitoring. In this work, we propose a semi-automatic envelope-based heart sounds identification method called the Largest Interval Heart Sounds Detection (LiHSD) that exploits the superiority of the Complete Ensemble Empirical Mode Decomposition with Adaptive Noise (CEEMDAN) and the cubic spline interpolation to discover several heart sounds' components such as period and location of S1 and S2, an interval of a cardiac cycle, and to obtain the duration and location of murmurs. Evaluation of the proposed system over several life sample data showed promising results comparable to the previous models. The algorithm was able to capture the largest interval of S1 and S2. The examination for normal heart sounds exhibited detection accuracy 98%, whereas for anomaly heart sounds samples the detection accuracy ranging from 89% to 97.5%. Furthermore, the proposed system has been successfully implemented in a real Internet of Things device while eyeing its contribution to the future of the smart healthcare system.**

***Index Terms*—Internet of Things, phonocardiography, signal detection, system identification, telemedicine.**

I. INTRODUCTION

The proliferation of healthcare-related sensors and communication networks technologies has successfully fostered the emergence of long-distance measurement and monitoring by way of the Internet of Things (IoT) [1-5]. This measurement and monitoring may include several human vital signs such as body temperature, blood pressure, heart rate, and respiratory rate [6]. Previous studies showed that this long-distance teleauscultation system shows promising results for the future telehealthcare system owing to several reasons. First, accurate sensors reading at the front end of the system may compensate for the lack of accuracy in human eye reading and interpretation. Secondly, the implementation of this Internet of Things assisted healthcare system can potentially reduce operational cost and time including doctor consultation, registration, and hospital queue as well as transportation. Lastly, the presence of the Internet of Things for healthcare in the developed countries may remove the medical care requirement gap between patients who live in isolated/remote areas and doctors in urban areas. In addition to that, must-have features which accompany a robust healthcare IoT development, like standards [7-9], architecture [5], protocols [2], and security [10-11] have been addressed thoroughly by industries and researches to create mature smart healthcare systems in the future.

Biologically, a normal heart produces two subsequent signals namely the first sound (S1) and the second sound (S2). The interval between S1 and S2 is the systole period, and the interval between S2 and the following S1 is the diastole phase. Hence, the term fundamental heart sound signals refer to the first and the second (S1 and S2, respectively) sounds that are mostly used for clinical assessment based on the phonocardiogram (PCG) procedure. It is well understood in the medical world that one-cycle fundamental heart sound signals normally elapse for 0.8 seconds period. Besides those S1 and S2 signals, other sounds like S3 (early diastolic heart sound), S4 (late diastolic heart sound), and murmurs may appear in the PCG. The S3 and S4 may occur in normal heart or may be associated with pathological activities. On the other hand, the murmurs that are triggered by structural and functional defects of the heart [12], mostly considered as abnormal clinical conditions of the heart.

Fig. 1 shows an example of a two-cycle normal heart sound signal in the top part of the figure and a two-cycle anomaly heart sound signal in the bottom part. The anomaly is shown in the bottom part of the figure commonly refers to as the *early systolic murmurs.* In this case, murmurs appear in the early systolic phase of heart sounds due to acute mitral regurgitation. These murmurs appear due to long vibrations that occur during the systole period because of turbulent blood flow through a partially obstructed opening mitral or tricuspid valves. Therefore, the presence of murmurs in the series of heart sounds can be an indication of abnormalities in the heart. Nevertheless, the duration and location of the murmurs may vary from one case to another make it difficult and complicated to identify the presence of murmurs in the heart sounds signal.

This study presents a method to extract important heart sounds signal components i.e. S1 and S2 as well as murmurs, followed by identification processes. The goal of the identification processes in this work is to determine: (i) the largest interval of S1, i.e. $T1$ and the largest interval of S2, i.e. $T2$, (ii) duration between S1 and the next S1 in the subsequent cardiac cycle, $T11$, (iii) duration between S1 and S2 in the same cardiac cycle, $T12$, and (iv) to obtain the duration of murmurs, T_{mur}, and their location. The

This work was supported by the Competitive Grant Fundamental Research, Minister of Research Technology and Higher Education, Republic of Indonesia (Number: 229/SP2H/LT/DRPM/2019).

Digital Object Identifier 10.4316/AECE.2021.01005

identification results together with the original PCG signals are then transmitted via Internet communication networks to be stored in a cloud system that allows doctors or experts to access them online anywhere for 24/7.

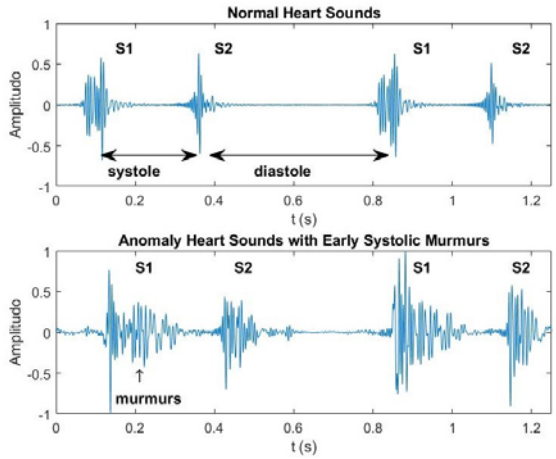

Figure 1. PCG signal for the normal (Sample01) and anomaly heart sounds with *early systolic murmur* (Sample09)

We introduce a successive procedure called the Largest Interval Heart Sound Detection (LiHSD) comprising three major steps. Firstly, in the pre-processing step, we employed a band-pass filter to the heart sounds and the Complete Ensemble Empirical Mode Decomposition with Adaptive Noise (CEEMDAN) to decompose the heart sounds. Subsequently, the CEEMDAN assisted with the Pearson distance metric was applied to separate the fundamental heart sounds, murmurs, and any unwanted signals. The separation process involved human perception to assist the decision; hence the term semi-automatic is applied in this paper. Finally, we exploited the cubic spline interpolation to leverage the quality of the data points in the segmented heart sound signals. Then based on the segmented cubic spline envelope, the various interested heart sounds parameters were determined.

The paper is organized according to the following sections. The first section serves as an introduction and problem definition that have driven the whole study presented in the paper. Section 2 describes a general framework of a teleauscultation system and related works in heart sound signals identification. Section 3 presents the proposed LiHSD model. It is then followed by results and analysis in Section 4. Finally, conclusions will be drawn in the last section.

II. Related Works

Several studies showed that phonocardiography signals are inherently complex, highly non-stationarity [13], and affected by a wide range of artifacts, which often lead to erroneous judgment towards the heart condition. In response to that, many of the research efforts have been carried out to the exploration of signal processing techniques to reduce its noise sensitivity and to improve the identification of heart sound signals to provide more reliable diagnostic tools.

Along with the proliferation of communications technology in the form of the Internet of Things (IoT), teleauscultation techniques coupled with heart sounds identification methods are growing fast to develop a complete smart healthcare system that enables people and medical services to monitor patients' heart condition remotely [1], [14-17].

Heart sounds identification requires several processes including denoising and signal segmentation. The latest deserves a considerable amount of research effort and advanced signal processing methods to produce a robust yet less time-consuming segmentation [18]. Some suggested works in the heart sounds identification algorithms relied on the envelop extraction techniques. For instance, the paper in [19] utilized the average Shannon energy normalization implemented for PCG signals. The study proposed Shannon energy as a key process in their identification method by exploiting the natural behavior of the Shannon energy in which it amplifies the medium intensity of the heart sound signals and at the same time attenuates the low-intensity signal. In this work, a threshold value was set up manually to separate noise and the fundamental heart sound signals. Even though the algorithm claimed that it achieved a success ratio of 93%, the paper showed that it only worked well for identifying normal heart sound signals.

The work in [20] investigated and examined several envelope extraction algorithms to identify the envelope curves of the first heart sounds, S1, and the second heart sounds, S2. Evaluation based on the segmentation rate showed three envelope extraction algorithms including the Shannon energy envelope, the Hilbert envelope, and the Cardiac sound characteristic waveform (CSCW) were able to give valid segmentation of the S1 and S2 signals for both normal and abnormal heart sound signals.

An interesting approach for the time-domain heart sounds identification was elaborated in [21]. It provided a different angle point of view by emphasizing the identification time occurrence of the two main components of the heart sound signals as well as its duration. The method required simultaneous measurement and recording of the ECG and PCG signals. The study showed a success rate of 99.2% of heart sound components identification.

Despite the popularity of the aforementioned time-domain envelope extraction methods, some literature showed that the frequency and time-frequency domain approaches might also work well for the identification of the heart sound signals. For example, the frequency domain analysis includes the fast Fourier transform (FFT) and the Mel Frequency Cepstral Coefficients (MFCC) techniques [18] whereas the time-frequency domain analysis employed several methods such as Wavelet [22-23], Hilbert Transform [24], Empirical Mode Decomposition (EMD) algorithms [14], and Deep Neural Networks [27-28]. However, several studies showed that the time-domain analysis might provide promising results in detecting the presence of murmurs compared to frequency-domain approaches.

Other studies exemplified the usefulness of the Hilbert Huang Transformation (HHT) in the pre-processing stage of heart sound identification [1]. In this work, the Empirical Mode Decomposition (EMD) separates the heart sound signals contaminated with noise and murmurs by firstly extracting them into a set of mono-component signals and then carefully selecting the most appropriate Intrinsic Mode Functions (IMFs) to represent the undistorted fundamental heart sound signals. Furthermore, a paper in [14] used the

later development of the EMD, i.e., the Complete Ensemble Empirical Mode Decomposition with Adaptive Noise (CEEMDAN) to identify the presence of murmurs in the heart sound signals. The CEEMDAN algorithm theoretically offers better spectral separation than the EMD method and at the same time, it overcomes the mode mixing problems occurring in the EMD method.

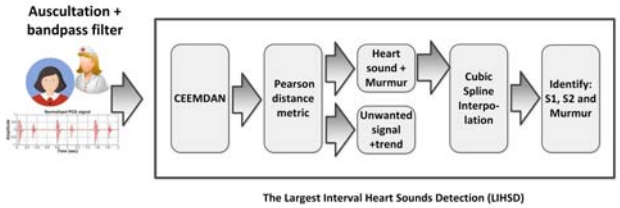

Figure 2. Proposed model of the Largest Interval Heart Sounds Detection (LiHSD)

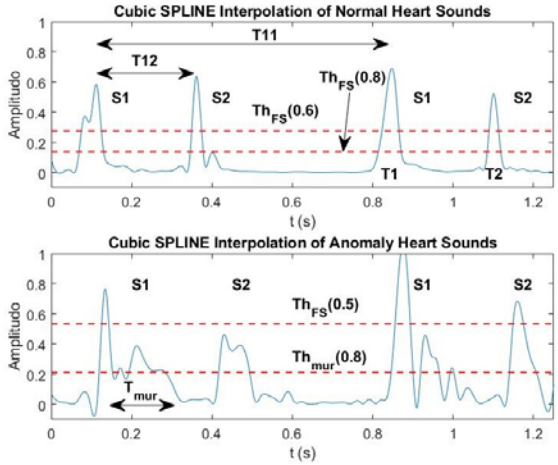

Figure 3. Cubic spline interpolation of normal heart sounds (Sample01) and anomaly heart sounds with *early systolic murmur* (Sample09). The dotted lines are thresholds

III. The Proposed Identification Method

Fig. 2 displays a block diagram containing modules of the proposed LiHSD heart sound identification method. Signal samples are usually captured using a digital stethoscope referring to the specific medical terms called auscultation. The identification process involves three subsequent procedures, i.e. pre-processing, separation of the fundamental heart sound signals and its murmurs, and followed by identification of heart sounds' parameters.

The main objective of the proposed method is to obtain the largest interval for S1, S2, and murmurs. This is motivated by the fact that these intervals provide significant diagnostic importance for the heart, for example, the long duration of both S1 and S2 signals could be a sign of heart abnormality. Previous methods in [1] and [24] utilized one or two threshold lines to determine the intervals. By comparing $Th_{FS}(0.8)$ and $Th_{FS}(0.6)$ in the top row of Fig.3, it is clear that the intervals of S1 and S2 may change depending on the position of the selected thresholds. When the threshold was set to 60% of the highest peak i.e. $Th_{FS}(0.6)$, it might only get a suboptimal length of the intervals. On the other hand, setting the threshold to 80% of the highest peak i.e. $Th_{FS}(0.8)$ might obtain the largest interval of S1 and S2. For the case of normal heart sounds, it is possible to place a threshold at a very low level of the envelope to get the largest crossing interval of both S1 and S2. For example, in the figure, the threshold was set to 80% of the highest peak, i.e. $Th_{FS}(0.8)$. Unfortunately, the same threshold position cannot be applied for heart sounds that are perturbed by murmurs. See the bottom part of Fig. 3. In this case, the setting threshold at a low level may give a wrong estimation of S1 and S2 intervals. Hence, to get a proper measurement of the intervals, the Th_{FS} was shifted higher at 50% and the Th_{mur} was set to 80% of the highest peak.

In this section, we describe a new model that will attempt to determine the largest interval measurement of the heart sounds components i.e. *T1*, *T2*, and T_{mur}.

A. Preprocessing

During the recording activities, heart sounds might be corrupted by various external or internal noise sources. Another type of artifacts that reside in the low-frequency range is the baseline wander arising from breathing, subject movement, speech, and digestion. Consequently, a band-pass Butterworth filter for a frequency range 50-400Hz was applied in the pre-processing phase to minimize the effect of those sources of noise on the targeted heart sounds.

Next, the system employs the CEEMDAN algorithm to decompose heart sound signals through sifting processes into a finite and small number of Intrinsic Mode Function (IMF) components. The resulting IMFs are time-varying single-frequency components that represent a set of basis functions for the heart sound signals [29–31]. Hence, as a result of the time domain decomposition process, an observed signal can be expressed mathematically as:

$$s(n)=\sum_{k=1}^{K}\overline{IMF}_k(n) \tag{1}$$

where, $\overline{IMF}_k(n)$ is the k-th IMF, and $\overline{IMF}_K(n)$is the trend-like final residue. Here, each of the k-th IMF components is an average of IMF_k over an ensemble of I trials the observed signals plus white Gaussian noise series with finite variance, that is in the mathematical form expressed as $\{s^i(n)=s(n)+\beta w^i(n)\}$, where the $\{w^i(n), i=1,\cdots,I\}$ indicates I realizations of the zero-mean unit variance white Gaussian noise series and β is the controlled noise amplitude. Therefore, the term $\overline{IMF}_k(n)$ represents the average of $\{IMF_k^i(n), i=1,\cdots,I\}$. Here we define heart sound signals as N-sample signals and denoted as $\{s(n), n=1,\cdots,N\}$, which is obtained through the process of recording an acoustic wave from a stethoscope.

The time-domain decomposition using CEEMDAN has advantages in increasing the possibility of the fundamental heart sound signals' components, the S1 and S2 to be distinguished from the other unwanted components, such as noise and murmurs. This pre-processing phase is particularly essential to extract the feature of not only anomaly heart sounds that mostly contains those non-stationary signals, but it is also useful for the normal heart sound signals that may comprise of several other signals and noise as a result of unclean auscultation process.

In a time-domain view, each IMF shows different oscillation waves from fast to slow as can be seen in Fig. 5. In this way, the CEEMDAN algorithm distributes the heart sounds frequency components across different IMFs. For

example, $\overline{IMF}_1(n)$ signifies the fastest oscillation whereas the highest subscription index has the slowest oscillation. The fundamental heart sound signals that are accompanied by murmur components (categorized as the pathological heart sounds) usually reside in several middle subscription indexes of the *k*-th IMFs.

B. Heart sounds separation

However, finding the exact IMFs that correspond to the fundamental heart sounds or murmurs only is obviously a challenging task, since there is no information about the frequency component contained in each IMF. Nevertheless, the detection of the fundamental heart sounds interval length heavily depends on the accurate execution in this step. Our proposed work in [14] suggested the use of the Pearson distance metric to separate noise and murmurs from the fundamental heart sound signals.

Pearson's correlation criteria that differentiate IMFs of the heart sound components is expressed according to (2),

$$d_k = \frac{\mathrm{cov}\left(s(n), \overline{IMF}_k(n)\right)}{\sqrt{\mathrm{cov}(s(n)).\mathrm{cov}\left(\overline{IMF}_k(n)\right)}} \tag{2}$$

where, d_k is the correlation coefficient that is associated with the $\overline{IMF}_k(n)$. Equation (2) clearly shows that the correlation coefficient is a cross-correlation between original signals and the $\overline{IMF}_k(n)$. Hence, the correlation coefficient represents the degree of similarity between original signals and each of the $\overline{IMF}_k(n)$. The denominator in the expression above serves to normalize the correlation coefficients such that $0 \le |d_k| \le 1$. Furthermore, the Pearson distance metric in (3) was proposed to describe the degree of similarity in a more meaningful way as it will be explained in the following paragraph.

$$p_k = 1 - |d_k| \tag{3}$$

The Pearson distance metric in (3) signifies the following logic: the smaller value of the Pearson distance metric implies a close distance (close similarity) between the originals signals and the $\overline{IMF}_k(n)$. In contrast, the highest value of the Pearson distance metric indicates that the two series are different.

1) Heart sounds without murmurs

The Pearson distance metric, p_k, in (3), is expected to serve as a proper threshold for IMF modes separation. For example, for the case of heart sounds without murmurs, our preliminary experiment showed when $\overline{IMF}_k(n)$ for $k = 1,2,\cdots,K_{FS}$ that are associated with $p_k \le 0.8$ are taken, then summing up all of the $\overline{IMF}_k(n)$ for $k = 1,2,\cdots,K_{FS}$ signifies the fundamental heart sound signals. On the other hand, all of the other $\overline{IMF}_k(n)$ for $k = K_{FS}+1,\cdots,K$ represents the modes that are involved in the construction of the extracted unwanted signals. The mathematical formulation for heart sounds separation is shown in (4)-(6).

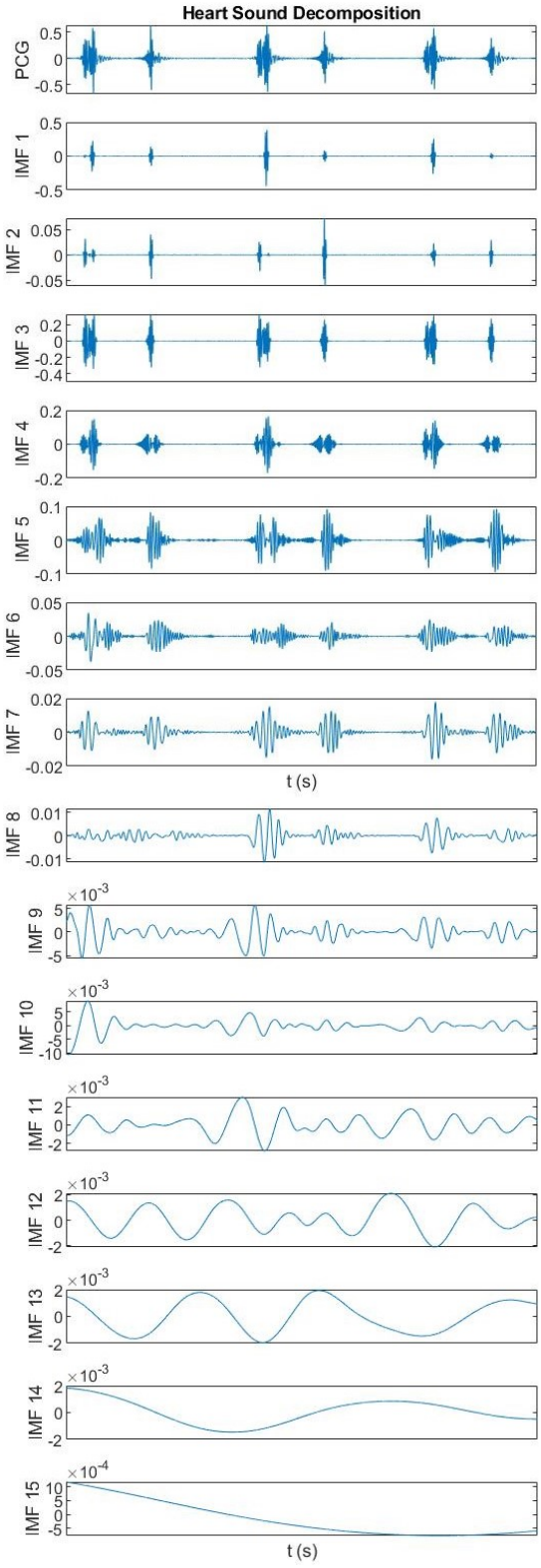

Figure 4. Decomposition of normal heart sounds (Sample01) using the CEEMDAN algorithm with $\beta = 0.1$ and $I = 100$

$$s(n) = y_{FS}(n) + y_{rem}(n) \tag{4}$$

$$y_{FS}(n) = \sum_{k=1}^{K_{FS}} \overline{IMF}_k(n), \qquad p_k \le 0.8 \tag{5}$$

$$y_{rem}(n) = \sum_{k=K_{FS}+1}^{K} \overline{IMF}_k(n), \qquad p_k > 0.8 \tag{6}$$

where, $y_{FS}(n)$ denotes the separated fundamental heart sound signals whereas $y_{rem}(n)$ signifies the extracted remaining unwanted signal and trend. Based on (6), the

main task of the algorithm is to select a series of $\overline{IMF}_k(n)$, which has Pearson distance smaller than or equal to 0.8 for $k = K_{FS}+1,\cdots,K$ to acquire the undistorted fundamental heart sounds.

Fig. 4 depicts the decomposition of normal heart sounds by using the CEEMDAN algorithm. In the figure, the normal heart sounds decompose into 15 independent IMFs. The IMFs with low subscription index indicate fast oscillation signals whereas the IMFs with high subscription indexes signify slow oscillation. Looking at the Pearson distance metric fluctuation against k in the second graph of Fig. 5, the IMFs that satisfy $p_k \le 0.8$ as in (5) are $\overline{IMF}_1(n),\cdots,\overline{IMF}_5(n)$. The extracted fundamental heart sounds, $y_{FS}(n)$ as a result of summing those IMFs is shown in the third figure of Fig. 5 and the separated unwanted signal, $y_{rem}(n)$, is shown in the bottom part of Fig. 5.

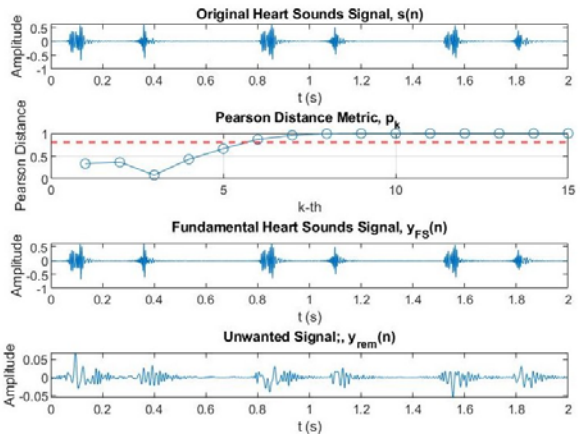

Figure 5. The original normal heart sounds (Sample01), the Pearson distance metric, the separated fundamental heart sounds, and the separated unwanted signals, respectively

2) Heart sounds with murmurs

The second case that is more intriguing than the type of heart sounds in the previous sub-section is the case for anomaly heart sounds with murmurs. Indeed, there have been several works attempting to separate fundamental heart sounds and murmurs, for example, the works in [1], [24-26]. However, due to the nature of murmurs: despites its non-stationarity, it also consumes a wide range of frequency from as low as 125 Hz to 250 Hz, the location of murmurs is varied across one cycle of heart sound signal, and their intensity can be benign or strong. As such, it makes no significant works are able to segment the murmurs completely. If they achieved significant results in separating murmurs, they mostly operated synthetic heart sound signals for evaluation of their proposed methods.

As there is no easy way to separate murmurs, in this work we entrust the choice of the targeted IMFs that construct the fundamental heart sounds or murmurs to the expert judgment based on the eye observation on the display of heart sounds' IMFs. Modification of (4) to (6) for the case of heart sounds with murmurs can be rewritten as in (7) to (10).

$$s(n) = y_{FS}(n) + y_{mur}(n) + y_{rem}(n) \tag{7}$$

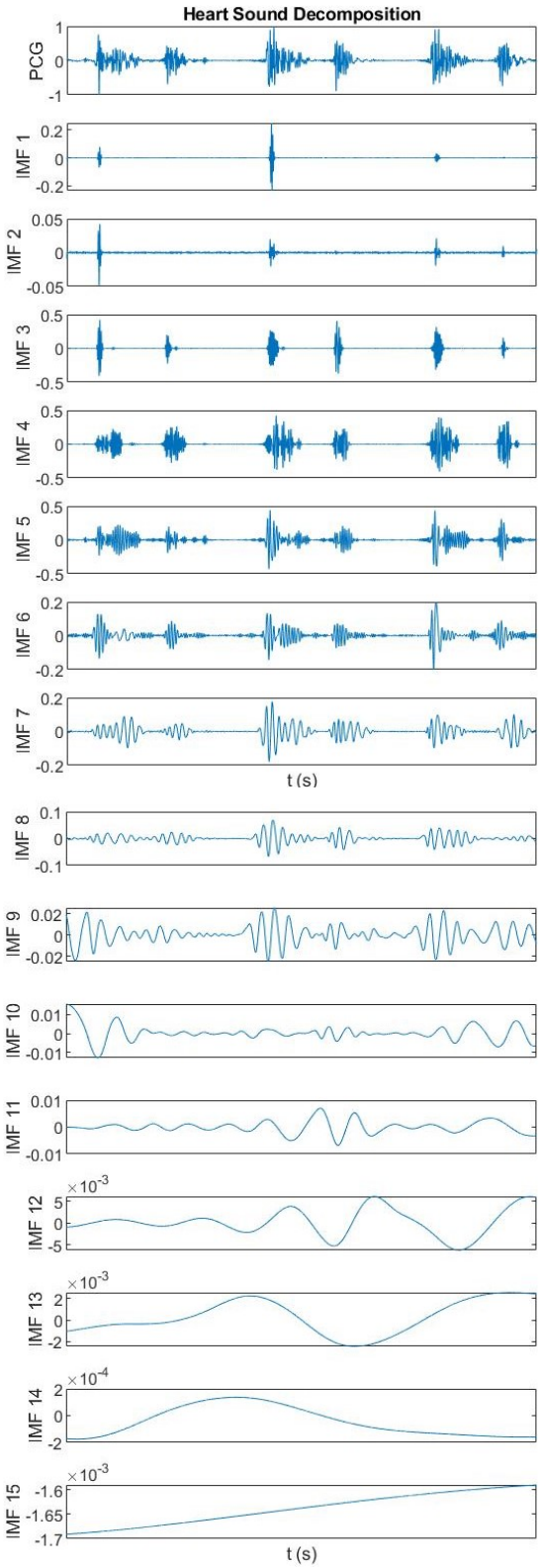

Figure 6. Decomposition of anomaly heart sounds (Sample09) using the CEEMDAN algorithm with $\beta = 0.1$ and $I = 100$

$$y_{FS}(n) = \sum_{k=1}^{K_{FS}} \overline{IMF}_k(n), \tag{8}$$

for K_{FS} based on expert judgment,

$$y_{mur}(n) = \sum_{k=K_{FS}+1}^{K_{mur}} \overline{IMF}_k(n), \tag{9}$$

for K_{mur} based on expert judgment,

$$y_{rem}(n) = \sum_{k=K_{mur}+1}^{K} \overline{IMF}_k(n). \tag{10}$$

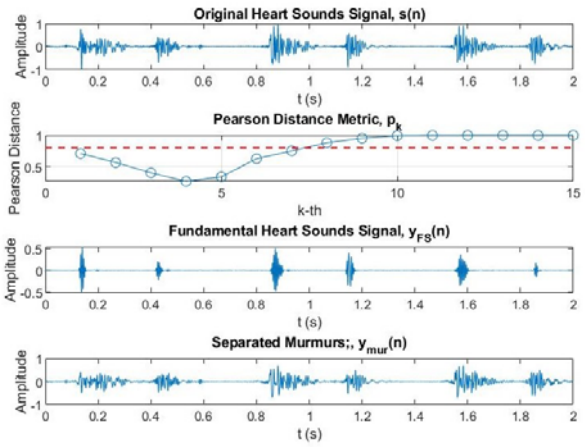

Figure 7. The original anomaly heart sounds with early systolic murmur (Sample09), the Pearson distance metric, the separated fundamental heart sounds, and the separated murmurs

For example, the decomposition of heart sounds with murmurs shown in Fig. 6 clearly indicates that the fundamental heart sounds, $y_{FS}(n)$, might be best represented by $\overline{IMF}_k(n)$ for $k=1,2,3$, whereas murmurs, $y_{mur}(n)$, might be satisfied by aggregating the $\overline{IMF}_k(n)$ for $k=4,\cdots,8$. Then the rest of IMFs are summed up to construct the remaining unwanted signal and trend. Fig. 7 displays the reconstruction of $\overline{IMF}_k(n)$ where the separated fundamental heart sounds, $y_{FS}(n)$ and the separated murmurs, $y_{mur}(n)$, can be seen in the last two rows of the figure. In this case, the Pearson distance metric shown in the second row of Fig. 7 serves as general guidance to choose the appropriate $\overline{IMF}_k(n)$ to characterize correct fundamental heart sounds representation, i.e., for a heart sound signal with murmurs, the fundamental heart sounds mostly can be reconstructed using several IMFs which have ks smaller than the kth of the lowest Pearson distance.

C. Heart sounds identification

In this step, we utilize the cubic spline interpolation to increase the detectability quality of the separated fundamental heart sounds and murmurs. This cubic spline interpolation fits all the heart sound signal's data points in some functions to improve the identification process for the heart sound components.

Given a set of $n+1$ data points (x_i, y_i) where $a=x_0<x_1<\cdots<x_n=b$ and no two x_i are the same, then the spline $S(x)$ defined as a function that satisfies $S(x)\in C^2[a,b]$. Furthermore, on each subinterval, $S(x)$ is a polynomial of degree 3 (cubic polynomial) and $S(x_i)=y_i$ for $i=1,2,\cdots,n$. The function $S(x)$ is represented compactly as in (11),

$$S(x)=\begin{cases} S_0(x), & (x_0\le x\le x_1),\\ S_1(x), & (x_1\le x\le x_2),\\ \vdots & \\ S_{n-1}(x), & (x_{n-1}\le x\le x_n). \end{cases} \tag{11}$$

A formula in (11) shows that cubic polynomials are joined together between x_0 and x_n to form the spline function. As each of $S_n(x)$ is a polynomial of degree 3, then it is clear that in this spline function discontinuities may occur in the third derivative; however such discontinuities are visually hard to detect using naked eyes. Thus, the cubic spline function may be able to represent the separated fundamental heart sound signals, $y_{FS}(n)$, the extracted murmurs, $y_{mur}(n)$, and the extracted unwanted signal, $y_{rem}(n)$, correctly.

After interpolation using the cubic spline, heart sounds interval detection will run according to the following steps (refer to parameters description in Fig. 3). Pseudocode representation of the algorithm can be seen in Appendix A.

a) Get the separated fundamental heart sounds data, $y_{FS}(n)$, and operate the cubic spline interpolation to get the heart sounds envelope, $\hat{y}_{FS}(n)$.

b) Set up a threshold value, Th_{FS}, for identifying the first (S1) and the second (S2) heart sounds according to (12).

$$Th_{FS}=a\times\max\left\{\hat{y}_{FS}(n)\right\} \tag{12}$$

where a is percentage relative to the envelope peak that is set to achieve the largest interval detection for both S1 and S2 and at the same time to eliminate very low-intensity unwanted signal, e.g. $a=90\%$. Therefore, the threshold setting is very important and may vary according to the operator choice.

c) Find all of the crossing points between heart sounds data and the Th_{FS}. Each of these two crossing points is the candidate for the S1 interval, $T1$, or the S2 interval, $T2$. See Fig. 4 for clarity. Then calculate the average value for each two data points to give the center position of all S1 and S2, say $M_{S1S2}(j)$, where $j=1,2,\cdots,J$ signifying consecutive S1 and S2.

d) Next, the algorithm decides the position of S1 or S2 based on basic principles: firstly, S1 and S2 are always in alternate order, and secondly, the interval between S1 and S2 is always narrower than the interval between S2 and S1. It is shown mathematically in (13) and (14).

$$\begin{aligned} &S1(j)=M_{S1S2}(j),\\ &\quad\text{if } M_{S1S2}(j+1)-M_{S1S2}(j)<\\ &\qquad M_{S1S2}(j+2)-M_{S1S2}(j+1) \end{aligned} \tag{13}$$

$$\begin{aligned} &S2(j)=M_{S1S2}(j),\\ &\quad\text{if } M_{S1S2}(j+1)-M_{S1S2}(j)>\\ &\qquad M_{S1S2}(j+2)-M_{S1S2}(j+1) \end{aligned} \tag{14}$$

e) Once the position of S1 and S2 has been determined, important components of heart sounds such as $T11$ and $T12$ can be derived as follows

$$\begin{aligned} T11(j)&=S1(j+1)-S1(j)\\ T12(j)&=S2(j)-S1(j) \end{aligned} \tag{15}$$

The last step in the proposed LIHSD algorithm is to discover the murmurs intervals, T_{mur}, and their position (for the case of heart sound signals with murmurs). Those parameters can be obtained using the following steps. See Appendix B for its pseudocode representation of the algorithm.

a) Get the separated murmurs data, $y_{mur}(n)$ and operate the cubic spline interpolation to get the murmurs envelope, $\hat{y}_{mur}(n)$.

b) Set up a threshold value, Th_{mur}, for identifying the murmurs according to (16).

$$Th_{mur} = b \times \max\{\hat{y}_{mur}(n)\} \quad (16)$$

where b is a percentage relative to the heart sounds envelope peak, e.g. $b = 80\%$. The threshold setting may vary according to the operator choice.

c) Determine all of the crossing points between $\hat{y}_{mur}(n)$ and the Th_{mur}. Assume that each of the furthest two crossing points is the $\tilde{T}_{mur}(j)$, and its location is relative to the position of $S1(j)$ and $S2(j)$. Therefore, $\tilde{T}_{mur}(j)$ is the interval of murmurs overlapped with $T1$ or $T2$. In fact, the overlapped position of murmurs gives a great advantage in deciding its location, whether it is a systolic murmur or diastolic murmur. Depend on the murmurs' position; its interval can be expressed mathematically according to (17) and (18).

$$T_{mur}(j) = \tilde{T}_{mur}(j) - T1(j), \quad \text{if } \tilde{T}_{mur}(j) \text{ overlap with } S1(j) \quad (17)$$

$$T_{mur}(j) = \tilde{T}_{mur}(j) - T2(j), \quad \text{if } \tilde{T}_{mur}(j) \text{ overlap with } S2(j) \quad (18)$$

IV. Results and Analysis

This section presents the results and analysis obtained by implementing the LiHSD algorithm in IoT devices. Each IoT device consists of a Raspberry Pi 3 Model B as a main processor connected to the Internet via WiFi. A Thinklabs One digital stethoscope with sampling frequency 8000 Hz was used to retrieve PCG signal from several people who have identified to have normal and anomaly heart sound signals.

In total, there are 50 samples of PCG signals taken from 11 volunteers, where each sample lasts at least 10 seconds periods. Therefore, there are 4950 heart sounds (cardiac) cycles involved in the examination. The volunteers consist of five women and six men with their ages ranging from 20 to 50 years old whereas three of them were indicated to have anomaly heart sounds. The process of taking PCG signals in this study is a non-invasive process, thus it did not involve any harmful procedure. However, privacy consent from all volunteers was sought before the signal retrieval. Additionally, in the experiment, we also utilized heart sound signals samples taken from the PhysioNet Challenge 2016 (particularly for heart sounds with anomaly) that are freely available on the Internet to validate the performance of the proposed LIHSD algorithm. The results in this study were obtained from applying those data to the proposed LiHSD algorithm, including the assessment in Table IV.

A. Implementation setup

The PCG data collected using a Thinklabs One digital stethoscope with a filter setting that enable it to take a signal in the frequency range between 50 Hz to 400 Hz. The stethoscope acts as an input sensor and a Raspberry Pi 3 Model B board was employed as the main signal processor for heart sounds identification. This single-board computer is considered capable enough to execute the proposed algorithm properly and at the same time, it gets the benefit of its small dimension. It has 4 x ARM Cortex-A53 CPU at speed 1.2 GHz and an IEEE 802.11n (WiFi) used for connecting the auscultation system to the global Internet cloud. After processing the signal, the Raspberry Pi subsequently transmits the data to a web application development cloud platform to allow the data to be accessed by particular healthcare services or doctors. Fig. 8 displays the front and rear view of the auscultation system. The PCG signal from each volunteer was taken on the mitral area in a sitting position as shown in Fig. 9 with careful supervision from a medical doctor.

Fig. 10 shows the captured heart sound signal waveforms from the mobile-based application as a function of time. These signal waveforms appear in the application interface of the healthcare services mobile devices that will serve as a decision support system for medical experts for further clinical evaluation. Fig. 10a represents normal heart sounds for the extracted fundamental signal and its cubic spline interpolation envelope, consecutively, whereas Fig. 10b shows anomaly heart sounds for the extracted fundamental signal and the cubic spline interpolation envelope.

Figure 8. An IoT node for the heart sounds auscultation and identification. Front view of the IoT node on the left side and rear view on the right side

Figure 9. Heart sounds auscultation in a sitting position

B. System evaluation

In this sub-section, we will elaborate on the evaluation of the proposed LiHSD algorithm into three categories including normal heart sound signals, anomaly heart sound signals without murmurs, and anomaly heart sound signals with murmurs. A comparison with existing algorithms and its limitation will be evaluated in the last part.

The normal heart sound waveform and their decomposition (for Sample01) have been shown in Fig. 4. Now based on (5) and the Pearson distance metric depicted in the second row of Fig. 6, we can see that $\overline{IMF}_1(n), \cdots, \overline{IMF}_5(n)$ are the best representation of the $y_{FS}(n)$. Reconstruction of $y_{FS}(n)$ and its envelope are shown in Fig. 11. In the figure the Th_{FS} was set to 90% to achieve the largest interval of $T1$ or $T2$. Once the cross points between the threshold and heart sound waveforms are

found, the LiHSD algorithm can now detect all components of the heart sounds according to (12) to (15) as shown in Table 1.

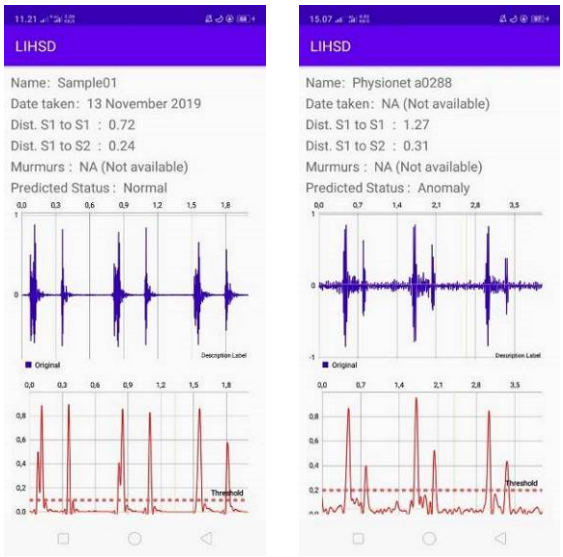

Figure 10. Mobile-based application signal waveform. Normal heart sounds (sample01) on the left side and anomaly heart sound (PhysioNet, a0288) on the right side

TABLE I. MEASUREMENT RESULTS OF THE NORMAL HEART SOUND COMPONENTS

Heart Sounds Components	Value
Number of cycles	2
Average of $T1$	83.8 ms
Average of $T2$	62.5 ms
$M_{S1S2}(1) = S1$	0.11 s
$M_{S1S2}(2) = S2$	0.37 s
$M_{S1S2}(3) = S1$	0.85 s
$M_{S1S2}(4) = S2$	1.11 s
$M_{S1S2}(5) = S1$	1.56 s
$M_{S1S2}(6) = S2$	1.82 s
Average of $T11$	0.73 s
Average of $T12$	0.26 s

Table I shows the averaged intervals of S1 and S2 are 83.8 ms and 62.5 ms, respectively. Particularly for S1, Fig. 11 shows that this interval comprises the split sound of the mitral and tricuspid valves closure. One of the indications for heart sounds normality is the interval or distance from S1 to S1 in the next cardiac cycles, and interval or distance from S1 to S2. The LiHSD algorithm detects their average as 0.73s for $T11$ and 0.26s for $T12$. This is an indication of normal heart sounds for Sample01. Examination results of normal heart sound for all samples are presented in Table IV.

Next, we will evaluate the anomaly heart sounds signal without murmurs. There are various indications of anomaly heart sounds in medical terms, such as longer or shorter duration of cardiac cycles and appearance of the third signal (S3), the fourth signal (S4), or murmurs in the heart sound signals. Here, we show examination for anomaly heart sound signals with a longer duration of cardiac cycles only. Examination of the other type anomaly heart sounds is elaborated in Table IV.

The third row of Fig. 12 depicts a reconstruction of a two-cycle heart sound signal that was taken from PhysioNet challenge 2016 database, i.e. a0288 signal. This extracted fundamental heart sounds in the third row is a result of aggregation $\overline{IMF}_3(n),\cdots,\overline{IMF}_6(n)$ corresponding to the Pearson distance metric $p_k \le 0.8$ as shown in the second row of Fig. 12.

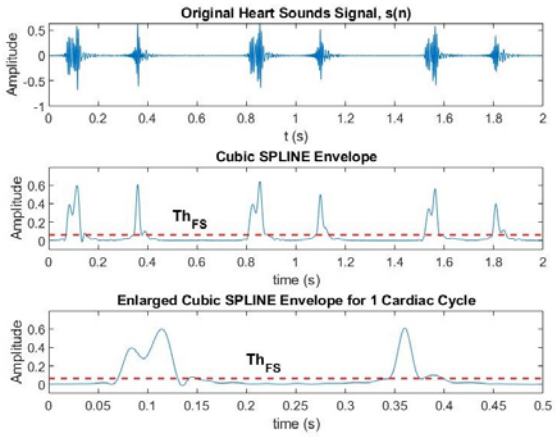

Figure 11. Extraction of normal heart sounds (Sample01). The dotted lines are thresholds set to 90% of the maximum peaks

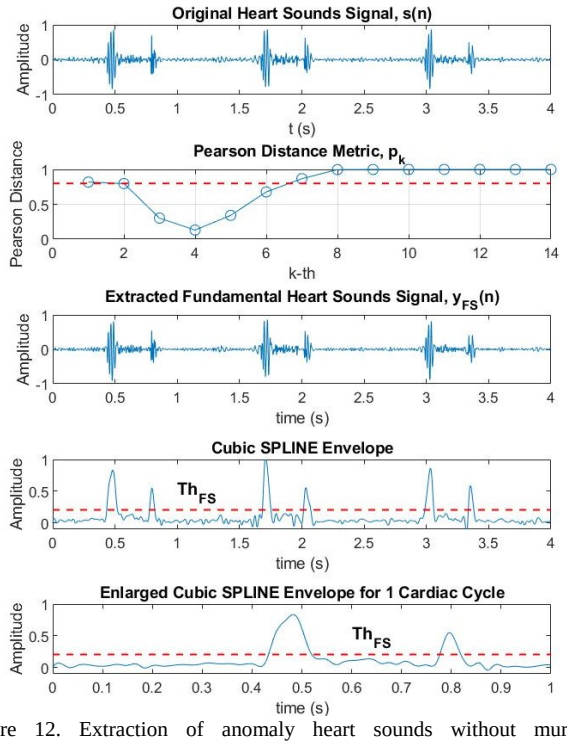

Figure 12. Extraction of anomaly heart sounds without murmurs (PhysioNet a0288). The dotted lines are thresholds set to 80% of the maximum peaks

We constructed a heart sounds envelope using the cubic spline interpolation and set the threshold Th_{FS} to 80%. The threshold was set a little bit higher in this type of heart sounds to eliminate the effect of low-intensity unwanted signals.

Table II enlists the measurement results of the targeted heart sound signals. Based on the results, it can be observed that the distance between two S1 signals or usually called 1 cardiac cycle is longer than the normal one. Here the $T11$ is equal to 1.27s. Indeed, a longer duration of $T11$ is an indication of a slower heart rate of a person than a normal adult human [27]. On the other hand, the interval between S1 and S2 is similar to the normal heart sounds, where $T12$

is 0.31s. It can also be noticed that for the case of this anomaly, the detected largest interval of S1 and S2 are both similar to the ones of the normal case.

TABLE II. MEASUREMENT RESULTS OF THE ANOMALY HEART SOUNDS WITHOUT MURMUR COMPONENTS

Heart Sounds Components	Value
Number of cycles	2
Average of $T1$	114 ms
Average of $T2$	53,5 ms
$M_{S1S2}(1)=S1$	0.48 s
$M_{S1S2}(2)=S2$	0.80 s
$M_{S1S2}(3)=S1$	1.72 s
$M_{S1S2}(4)=S2$	2.04 s
$M_{S1S2}(5)=S1$	3.07 s
$M_{S1S2}(6)=S2$	3.36 s
Average of $T11$	1.27 s
Average of $T12$	0.31 s

Lastly, we will show an examination of the proposed algorithm for identifying heart sound signals with murmurs. Fig. 6 observes the decomposition of heart sounds with systolic murmurs that were recorded from Sample09. Subsequently, extraction of the heart sounds is shown in Fig. 13. The procedure to detect the heart sounds' components comprised of two steps, as explained in sub-section III.C., i.e., detection of fundamental heart sound signals' components and detection of murmurs characteristics. Measurement results obtained by the LiHSD algorithm are shown in Table IV.

Due to the nature of the CEEMDAN algorithm in Fig. 6, the fundamental heart sounds, $y_{FS}(n)$, can be reconstructed by using $\overline{IMF}_k(n)$ for $k=1,2,3$. As a result of this reconstruction, the detected average interval of $T1$ and $T2$ are noticeably narrower than the ones of the normal heart sounds. However, the average interval of one cardiac cycle shown in Table III as $T11$ is considerably similar to the normal heart sounds.

Extraction of murmurs, $y_{mur}(n)$, shown in the fourth row of Fig. 13 was a result of reconstruction the $\overline{IMF}_k(n)$ for $k=4,\cdots,8$. Comparing the enlarged envelope fundamental heart sounds representation in the third row of Fig. 13 and the enlarged envelope depiction of murmurs in the bottom row, it is clearly seen that the position of murmurs overlies the position of the fundamental heart sounds envelope. Therefore, the interval of murmurs, $T_{mur}(j)$, can be obtained by subtracting the duration of its counterpart $T1$ or $T2$ from $T'_{mur}(j)$ as shown in (16). The detected average duration of T_{mur} is enlisted in Table III.

Table III shows that the LiHSD algorithm is able to detect both the systolic and diastolic murmurs. Nevertheless, the systolic murmurs occupy almost 50% of the systole interval whereas the diastolic murmurs reside in only 4% of the diastole period. Because the occupation of murmurs in the diastole area is minor (e.g., under 20%), we chose not to include the diastole murmurs in the detected location of the murmurs. This is the reason why the last row of Table III displays the location of murmurs as systole.

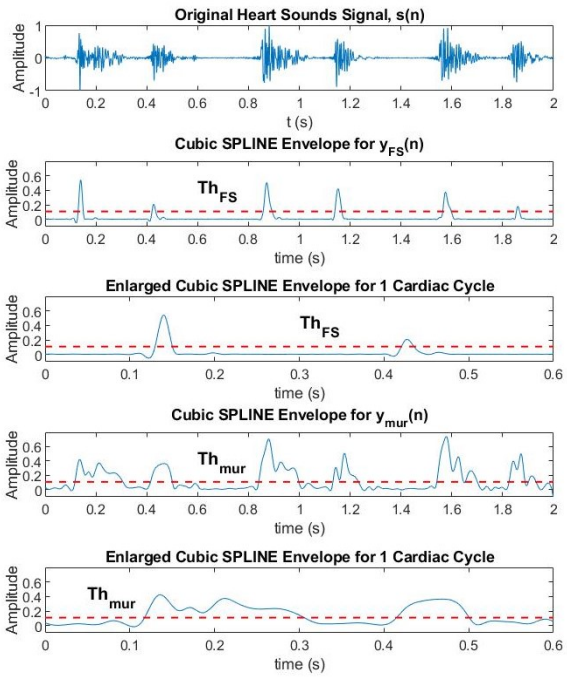

Figure 13. Extraction of anomaly heart sounds with systolic murmur (Sample09). The dotted lines are thresholds set to 80% of the maximum peaks

TABLE III. MEASUREMENT RESULTS OF THE ANOMALY HEART SOUNDS WITH EARLY SYSTOLIC MURMUR COMPONENTS

Heart Sounds Components	Value
Number of cycles	2
Average of $T1$	36.4 ms
Average of $T2$	24,6 ms
$M_{S1S2}(1)=S1$	0.14 s
$M_{S1S2}(2)=S2$	0.43 s
$M_{S1S2}(3)=S1$	0.88 s
$M_{S1S2}(4)=S2$	1.15 s
$M_{S1S2}(5)=S1$	1.58 s
$M_{S1S2}(6)=S2$	1.86 s
Average of $T11$	0.72 s
Average of $T12$	0.28 s
Average of $\tilde{T}_{mur}$	Systole: 0.16 s Diastole: 0.09 s
Average of T_{mur}	Systole: 0.12 s Diastole: 0.03 s
Murmurs location	Systole

C. Limitation of the LiHSD algorithm

Detection of pathological heart sounds with an indication of murmurs in this study can be considered as the most challenging task among other types of anomaly heart sounds. This is mainly due to the wide range frequency content of murmurs that sometimes cannot be differentiated from S1 or S2 signals [32]. For example, Fig. 14 exhibits the spectrum of the heart sounds with systolic murmurs of Sample09 over a frequency range of 0-1000Hz. The figure clearly indicates that the fundamental heart sounds (Fig. 14b) and the murmurs (Fig. 14c) occupy the same spectrum, particularly at 100-200 Hz.

Fig. 15 shows an anomaly heart sound with *aortic stenosis murmur*. The figure displays the decomposition of the sample a0002 heart sounds taken from PhysioNet database. In this case, the extraction of fundamental heart sounds and murmurs using the CEEMDAN was utterly unsuccessful. For example, there are no possible IMFs that could be reconstructed to form fundamental heart sound

signals. Therefore, there is no way to detect the heart sound components for this kind of signal.

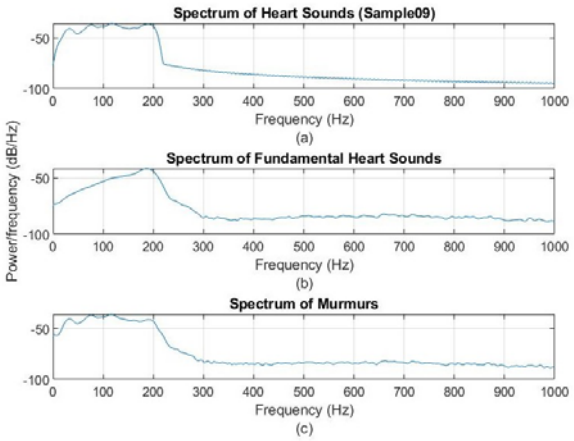

Figure 14. The spectrum of heart sounds (Sample09), fundamental heart sounds, and murmurs

D. Comparison of the LiHSD algorithm with existing methods

Finally, Table IV presents a comparative analysis of the proposed LiHSD algorithm with the existing envelope-based methods. The accuracy in the rightmost column in the table is a measure of the number of correct detection of S1, S2, and murmurs location for each cycle compared to the number of cardiac cycles involved in the experiment.

It can be noticed from the table that the proposed algorithm is able to capture the largest interval of the $T1$ and $T2$ compare with the existing algorithms in particular for normal heart sounds. More importantly, our proposed algorithm has been tested on real-time measurement heart sound signals whereas the other existing algorithms [24-26] were examined by utilizing the synthetic heart sound signals. Furthermore, the proposed LiHSD algorithm shows promising results in its detection accuracy, i.e. it detected the fundamental heart sounds' components with accuracy 98% for the normal heart sounds. However, the detection accuracy only ranging from 89% to 97.5% for the case of anomaly heart sounds. These are mainly due to two reasons. First, the non-stationary nature of the signal demands a not so easy method to extract the signal components. Second, murmurs might exhibit a wide range of frequency content that is sometimes overlapped with the frequency content of the fundamental heart sounds, i.e. S1 and S2. Therefore, it complicates the decomposition using the CEEMDAN algorithm, and hence, it obscures the reconstruction process to separate the fundamental heart sounds and their murmurs such as the one shown in Fig. 15.

V. CONCLUSION

In this work, we have proposed a semi-automatic envelope-based method for identifying components of heart sound signals. We called the Largest Interval Heart Sound Detection (LiHSD) algorithm. The LiHSD comprised several phases including pre-processing, heart sounds separation, and heart sound identification. The heart sounds separation process depended on the CEEMDAN algorithm assisted with the Pearson distance metric, whereas the cubic spline interpolation was employed in the last phase to improve the heart sound identification process.

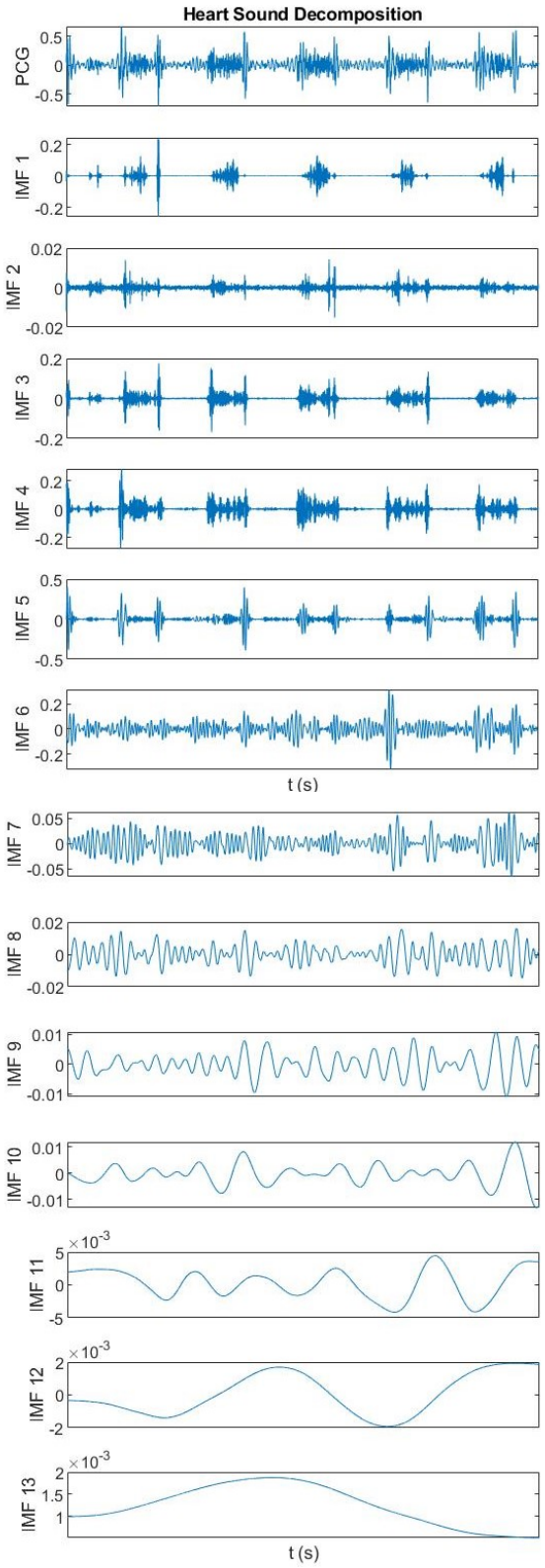

Figure 15. Decomposition of anomaly heart sounds with *aortic stenosis* murmur (PhysioNet database sample a0002) using the CEEMDAN algorithm with $\beta = 0.1$ and $I = 100$

Performance evaluation on the proposed system on the life heart sounds samples showed that the algorithm detected the largest interval of the $T1$ and $T2$. It also showed high detection accuracy compared to the previous models. The proposed model was able to detect the first and the second heart sounds for normal heart sounds with an accuracy of 98%. However, the detection accuracy ranging from 89% to 97.5% for the case of anomaly heart sounds. Particularly for heart sound signals with murmurs, the algorithm can only

detect the first and the second heart sounds properties with an accuracy of 89%. The proposed system has been successfully implemented in an Internet of Things device that is connected to the global Internet to allow long-distance measurement and monitoring, as we believe this model of medical examination will become the future of healthcare system.

TABLE IV. COMPARISON ANALYSIS

Method	$T1$ **(ms) (S1 interval)**	$T2$ **(ms) (S2 interval)**	$T11$ **(s) (Cardiac cycle)**	**Accuracy (%)**
LiHSD				
Normal heart sounds	84.2	61.3	0.82	98
Anomaly heart sounds:				
- Longer cardiac cycle	92.4	55.1	1.32	97.5
- Systolic murmur	37.5	25.6	0.75	89
- S3	84.2	54.2	0.84	97
- S4	84.0	35.6	0.84	95
SEPD [25]				
Normal heart sounds	22	16.1	0,70	S1:94.5 S2:92.2
Anomaly heart sounds	41.1	42.2	0.62	
Puspasari et al. [26]				
Normal heart sounds	NA	NA	0.81	84.9
Anomaly heart sounds:				
- Mitral regurgitation	NA	NA	0.94	
- Aortic stenosis	NA	NA	0.80	
- Mitral stenosis	NA	NA	1.02	
Atbi *et al.* [24]				
Normal heart sounds	62.3	48.1	0.78	NA
Anomaly heart sounds:				
- Systolic murmur	82.9	67.4	0.80	
- Opening snap	105	95.5	0.80	
- Diastolic murmur	67.3	48.5	0.80	

*NA: Not available

APPENDIX A

Algorithm 1. Pseudocode of the LiHSD algorithm to compute the *T1*, *T2* and *T11*.

```
% fs is the sampling frequency
% r is the decimation ratio
% pFS is the smallest number of points of the T1 or T2

yFS ← yECG;  % separated fundamental heart sound signal
yAposFS ← cubicSPLINE(yFS);
a ← input('Enter the threshold');
tH1 ← a*max(yAposFS);

% compute the crossing points
yRound ← round(yAposFS,1);
[idx,crossedPoint] ← find(yRound==tH1);

% compute the beginning and end of S1 and S2
length_idx ← length(idx);
idxKeep(1) ← idx(1);
j ← 2
for i ← 1:(length_idx-1)
   temp = idx(i+1)-idx(i);
   if temp>pFS
      idxKeep(j) ← idx(i);
      idxKeep(j+1) ← idx(i+1);
      j = j+2;
   end if
end for
idxKeep(end+1) ← idx(end);

idxKeep2 ← reshape(idxKeep,2,[]);
timeSpan ← (idxKeep2(2,:)-idxKeep2(1,:))/(fs/r);

% compute the center of the time span of S1 and S2
midTimeSpan ← idxKeep2(1,:)/(fs/r)+0.5*timeSpan;

% compute the averaged time span of S1 and S2
avgT1 ← mean(timeSpan(1:2:end));
avgT2 ← mean(timeSpan(2:2:end));

% compute the distance of S1 and S2
j ←0;
for i ← 2:length(midTimeSpan)
   j ← j+1;
   distS1S2(j) ← midTimeSpan(i)-midTimeSpan(i-1);
end for

% averaged distance
avgT12 ← mean(distS1S2(1:2:end));
avgT21 ← mean(distS1S2(2:2:end));
avgT11 ← avgS1S2 + avgS2S1;

% Labeling the fundamental signal as S1 or S2
for i ← 1:3
   S1 ← midTimeSpan(i+1) - midTimeSpan(i);
   S2 ← midTimeSpan(i+2) - midTimeSpan(i);
   if S1 < S2
      Sound(1:2:length(midTimeSpan)) ← "S1";
      Sound(2:2:length(midTimeSpan)) ← "S2";
   else
      Sound(1:2:length(midTimeSpan)) ← "S2";
      Sound(2:2:length(midTimeSpan)) ← "S1";
   End if
End for

% End of pseudocode
```

APPENDIX B

Algorithm 2. Pseudocode of the LiHSD algorithm to compute the T_{mur}.

```
% fs is the sampling frequency
% r is the decimation ratio
% pMur is the smallest number of points of the  T_mur

yMur ← yECGmur;  % separated murmurs
yAposMur ← cubicSPLINE(yMur);
b ← input('Enter the threshold');
tH2 ← b*max(yAposMur);

% compute the crossing points
yRound ← round(yAposMur,1);
[idx,crossedPoint] ← find(yRound==tH2);

% compute the beginning and end of the murmurs
length_idx ← length(idx);
idxKeep(1) ← idx(1);
j ← 2
for i ← 1:(length_idx-1)
   temp = idx(i+1)-idx(i);
   if temp>pMur
      idxKeep(j) ← idx(i);
      idxKeep(j+1) ← idx(i+1);
      j = j+2;
   end if
end for
idxKeep(end+1) ← idx(end);

idxKeep2 ← reshape(idxKeep,2,[]);
timeSpan ← (idxKeep2(2,:)-idxKeep2(1,:))/(fs/r);

% compute the averaged time span for the murmurs
avgMurT1 ← mean(timeSpan(1:2:end));
avgMurT2 ← mean(timeSpan(2:2:end));

% End of pseudocode
```

ACKNOWLEDGMENT

The research is funded by the Competitive Grant Fundamental Research, Minister of Research Technology and Higher Education, Republic of Indonesia (Number: 229/SP2H/LT/DRPM/2019). We also acknowledge great support from Eka Sari Oktarina (Laboratory Assistant) and two of our Bachelor Degree of Computer Engineering students, Zendi Zakaria Raga Permana (16410200033) and Miskiyanto (17410200044) for their endless available time in processing data.

REFERENCES

[1] H. Ren, H. Jin, C. Chen, H. Ghayvat, and W. Chen, "A novel cardiac auscultation monitoring system based on wireless sensing for healthcare," IEEE J. Transl. Eng. Heal. Med., vol. 6, no. April, pp. 1–12, 2018. doi:10.1109/JTEHM.2018.2847329

[2] S. B. Baker, W. Xiang, and I. Atkinson, "Internet of Things for smart healthcare: technologies, challenges, and opportunities," IEEE Access, vol. 5, pp. 26521–26544, 2017. doi:10.1109/ACCESS.2017.2775180

[3] Y. Yin, Y. Zeng, X. Chen, and Y. Fan, "The Internet of Things in healthcare: An overview," J. Ind. Inf. Integr., vol. 1, pp. 3–13, 2016. doi:10.1016/j.jii.2016.03.004

[4] J. Jusak and I. Puspasari, "Wireless tele-auscultation for phonocardiograph signal recording through Zigbee networks," in Proc. APWiMob 2015 - IEEE Asia Pacific Conf. Wirel. Mob., pp. 95–100, 2016. doi:10.1109/APWiMob.2015.7374939

[5] C. Rotariu, V. Manta, H. Costin, "Wireless remote monitoring System for patients with cardiac pacemakers," 2012 International Conference and Exposition on Electrical and Power Engineering (EPE), 2012, Iasi, Romania, pp: 845-848, Oct. 25-27, 2012, doi:10.1109/ICEPE.2012.6463828

[6] H. Costin, C. Rotariu, I. Alexa, et al., "TELEMON - A complex system for real time medical telemonitoring," 11th Int. Congress of the IUPESM/World Congress on Medical Physics and Biomedical Engineering, Munich, Germany, Sept. 07-12, Vol. 25, PT 5, Book Series: IFMBE Proceedings, pp.: 92-96, Part: 5, Published: 2009, doi:10.1007/978-3-642-03904-1_25

[7] A. Limaye and T. Adegbija, "HERMIT: A benchmark suite for the Internet of Medical Things," IEEE Internet of Things J., vol. 5, no. 5, pp. 4212–4222, 2018. doi:10.1109/JIOT.2018.2849859

[8] U.S. Department of Health and Human Services, "HIPAA security series: 1 security 101 for covered entities," Centers for Medicare & Medicade Sercices, vol. 2, pp. 1–11, 2007

[9] ***, The European Parliament and The Council of European Union, "Directive 95/46/EC of the European Parliament and of the council of 24 October 1995 on the protection of individuals with regard to the processing of personal data and on the free movement of such data," Official Journal L281, pp. 31-50, 1995

[10] J. Jusak and S.S. Mahmoud, "Novel and Low Processing Time ECG Security Method Suitable for Sensor Node Platforms," International Journal of Communication Networks and Information Security, vol. 10, no. 1, pp. 213–222, 2018

[11] K. H. Yeh, "A Secure IoT-based healthcare system with body sensor networks," IEEE Access, vol. 4, pp. 10288–10299, 2016. doi:10.1109/ACCESS.2016.2638038

[12] J. S. Coviello, Auscultation Skills: Breath & Heart Sounds, Wolters Kluwer Health, pp. 56-91, 2014

[13] A. K. Abbas and R. Bassam, Phonocardiography Signal Processing, Morgan & Claypool, pp. 13-18, 2009

[14] J. Jusak, I. Puspasari, and P. Susanto, "Heart murmurs extraction using the complete Ensemble Empirical Mode Decomposition and the Pearson distance metric," in Proc. 2016 Int. Conf. Inf. Commun. Technol. Syst. ICTS 2016, no. 058, pp. 140–145, 2017. doi:10.1109/ICTS.2016.7910288

[15] S. H. Kang, B. Joe, Y. Yoon, G. Y. Cho, I. Shin, and J. W. Suh, "Cardiac auscultation using smartphones: Pilot study," JMIR mHealth uHealth, vol. 6, no. 2, pp. 1-11, 2018. doi:10.2196/mhealth.8946

[16] K. V. I. Chatzakis and I. G. ssilakis, C. Lionis, "Electronic health record with computerized decision support tools for the purposes of a pediatric cardiovascular heart disease screening program in crete," Comput. Methods Programs Biomed., vol. 159, pp. 159–166, 2018. doi:10.1016/j.cmpb.2018.03.009

[17] I. S. Ateeq, K. Hameed, M. Khowaja, and S. H. Khan, "Design and implementation of digital tele stethoscope," in World Congress on Medical Physics and Biomedical Engineering 2018, 2019, pp. 867–873. doi:10.1007/978-981-10-9038-7_160

[18] S. Ismail, I. Siddiqi, and U. Akram, "Localization and classification of heart beats in phonocardiography signals —a comprehensive review," EURASIP J. Adv. Signal Process., vol. 2018, no. 1, 2018. doi:10.1186/s13634-018-0545-9

[19] H. Liang, S. Lukkarinen, and I. Hartimo, "Heart sounds segmentation algorithm based on heart sounds envelogram," Comput. Cardiol., no. October 1997, pp. 105–108, 1997. doi:10.1109/CIC.1997.647841

[20] S. Choi and Z. Jiang, "Comparison of envelope extraction algorithms for cardiac sound signal segmentation," Expert Syst. with Appl., vol. 34, no. 2, pp. 1056–1069, 2008. doi:10.1016/j.eswa.2006.12.015

[21] N. Giordano and M. Knaflitz, "A novel method for measuring the timing of heart sounds components through digital phonocardiography," Sensors, vol. 19, no. 8, pp. 1-16, 2019. doi:10.3390/s19081868

[22] V. N. Varghees, K.I Ramachandran, and K.P. Soman, "Wavelet-based fundamental heart sound recognition method using morphological and interval features," Healthcare Technology Letters, vol. 5, no. 3., pp. 81–87, 2018. doi:10.1049/htl.2016.0109

[23] B. Ergen, Y. Tatar, and H. O. Gulcur, "Time–frequency analysis of phonocardiogram signals using wavelet transform: a comparative study," Comput. Methods Biomech. Biomed. Engin., vol. 15, no. 4, pp. 371–381, 2012. doi:10.1080/10255842.2010.538386

[24] A. Atbi, S. M. Debbal, F. Meziani, and A. Meziane, "Separation of heart sounds and heart murmurs by Hilbert transform envelogram," J. Med. Eng. Technol., vol. 37, no. 6, pp. 375–387, 2013. doi:10.3109/03091902.2013.816379

[25] D. Mandal, A. Maity, and I.S. Misra, "Low cost portable solution for real-time complete detection and analysis of heart sound components," Wireless Personal Communications, vol. 107, pp. 523-547, 2019. doi:10.1007/s11277-019-06287-0

[26] I. Puspasari, W. I. Kusumawati, E. S. Oktarina and J. Jusak, "A New Heart Sound Signal Identification Approach Suitable for Smart Healthcare Systems," in 2019 2nd International Conference on Applied Engineering (ICAE), Batam, Indonesia, 2019, pp. 1-6, doi:10.1109/ICAE47758.2019.9221752

[27] F. Dong et al., "Machine listening for heart status monitoring: introducing and benchmarking HSS—The Heart Sounds Shenzhen Corpus," IEEE Journal of Biomedical and Health Informatics, vol. 24, no. 7, pp. 2082-2092, July 2020, doi:10.1109/JBHI.2019.2955281

[28] Krishnan, P.T., Balasubramanian, P., and Umapathy, S. "Automated heart sound classification system from unsegmented phonocardiogram (PCG) using deep neural network," Phys Eng Sci Med 43, pp. 505–515 2020. doi:10.1007/s13246-020-00851-w

[29] N. E. Huang et al., "The empirical mode decomposition and the Hilbert spectrum for nonlinear and non-stationary time series analysis," Proc. R. Soc. London. Ser. A Math. Phys. Eng. Sci., vol. 454, no. 1971, pp. 903–995, 1998. doi:10.1098/rspa.1998.0193

[30] M. E. Torres, M. A. Colominas, G. Schlotthauer, and P. Flandrin, "A complete ensemble empirical mode decomposition with adaptive noise," in 2011 IEEE International Conference on Acoustics, Speech and Signal Processing (ICASSP), 2011, pp. 4144–4147. doi:10.1109/ICASSP.2011.5947265

[31] M. A. Colominas, G. Schlotthauer, and M. E. Torres, "Improved complete ensemble EMD: A suitable tool for biomedical signal processing," Biomed. Signal Process. Control, vol. 14, no. 1, pp. 19–29, 2014. doi:10.1016/j.bspc.2014.06.009

[32] A. K. Dwivedi, S. A. Imtiaz, and E. R. Villegas, "Algorithms for automatic analysis and classification of heart sounds-a systematic review," IEEE Access, vol. 7, pp.8316-8345, 2019. doi:10.1109/ACCESS.2018.288943